

# Using Metamodeling and Fluid-Structure Interaction Analysis in Multi-Objective Optimization of a Butterfly Valve

Laura PAŁYS\*, Mirosław W. MRZYGŁÓD

*Faculty of Mechanical Engineering  
Opole University of Technology*

Mikołajczyka 5, 45-271 Opole, Poland; e-mail: m.mrzyglod@po.edu.pl

\*Corresponding Author e-mail: laura.palys@doktorant.po.edu.pl

Along with the increase in computing power, new possibilities for the use of parametric coupled analysis of fluid flow machines and metamodeling for many branches of industry and medicine have appeared. In this paper, the use of a new methodology for multi-objective optimization of a butterfly valve with the application of the fluid-structure interaction metamodel is presented. The optimization objective functions were to increase the value of the KV valve's flow coefficient while reducing the disk mass. Moreover, the equivalent von Mises stress was accepted as an additional constraint. The centred composite designs were used to plan the measuring point. Full second-order polynomials, non-parametric regression, Kriging metamodeling techniques were implemented. The optimization process was carried out using the multi-objectives genetic algorithm. For each metamodel, one of the optimization candidates was selected to verify its results. The best effect was obtained using the Kriging method. Optimization allowed to improve the KV value by 37.6%. The metamodeling process allows for the coupled analysis of the fluid flow machines in a shorter time, although its main application is geometry optimization.

**Keywords:** metamodeling, surrogate model, computational fluid dynamics, design of experiment, optimization, butterfly valve.

## NOTATION

CAD – computer-aided design,  
CCD – centered composite designs,  
CFD – computational fluid dynamics,  
DN – nominal diameter,  
DOE – design of experiment,  
FSI – fluid-structure interaction,  
GA – genetic algorithm,  
GEK – gradient-enhanced Kriging,  
KV – flow coefficient of a device,

LHS – Latin-hypercube sampling,  
MOGA – multi-objective genetic algorithm,  
NPR – non-parametric regression,  
NSGA-II – non-dominated sorted genetic algorithm-II,  
OA – orthogonal array,  
RSM – response surface method,  
 $y^+$  – non-dimensional wall distance.

## 1. INTRODUCTION

Improving fluid flow machinery design, its price, and reliability is necessary to meet the growing demands of the market. Along with the increase in computing power, new possibilities for the use of multi-objective optimization of such kind of equipment for many branches of industry and medicine have appeared. In this paper, the authors proposed a new multi-objective and multidisciplinary metamodeling methodology dedicated to fluid flow machines. The work is illustrated by an example of optimization of the butterfly valve design and operation based on a metamodeling framework.

In the past, the traditional approach to work on fluid flow machinery design was based on experience and ready-made solutions. The vision of a designer was limited in this research area. The development of numerical methods and their adaptation to various areas of engineering give much more possibilities for accomplishment in this field. Computational fluid dynamics (CFD) analysis software has been successfully used, meeting the scientific and industrial requirements in the design of butterfly valves. Their large number and the continuous improvement of the topic indicate a continued interest in this problem. In one of the earliest research [1], the authors point out that there is a certain relationship between the turbulence models and the correctness of the results, depending on its degree of opening. The most expensive models showed the greatest agreement, although most studies allow maintaining a balance between simulation time and accuracy of results. In another article [2] authors present a comparison of the experimental and simulation results of the flow coefficient for a butterfly valve, demonstrating the influence of the length of the inlet and outlet channels on the value of the estimation error. In the simulation described in [3], the authors investigated the effect of the location of the butterfly valve between two opposing 90° elbows. In their considerations, they use the analysis of torque fluctuations in the context of the possibility of transmission to mechanical vibrations. The possibilities of using numerical software in determining the noise of butterfly valves are presented in [4]. The next attempt to analyze the large butterfly valve is presented in [5], where authors show not only structural and fluid analyses but also indicate the need to change the shape of the disk. Performance between the single disk type butterfly valve and the double disk type

was investigated in [6]. Another example of simulation on the dependence of the disk shape and the dynamic-valve-torque is presented in [7]. Interesting solutions can be observed in the work [8], which presents research on a valve with a rectangular cross-section. Small size and cooling electrical device application, its cross-sectional area result in a more linear flow characteristic. The process of optimizing the butterfly valve design can be found in the publication [9]. Researchers utilized the Kriging surrogate model and orthogonal array for the design of experiment (DOE). Furthermore, in [10] the orthogonal array (OA) method and the quadratic response surface method (RSM) together with topology optimization of the butterfly valve are presented. Genetic algorithms were implemented in [11] for butterfly valve optimization.

Methods of experimenting were developed to systematize the study, especially those with a large number of variables. The design of experiment was officially implemented by Ronald A. Fisher in the 1920s, who researched agriculture. Collecting data was challenging, for this reason, it was necessary to systematize the way of obtaining results [12]. Searching for experimental points was the first stage of the procedure. The method of their selection depends on a few matters: a prediction error, the number of repetitions that can be performed, or the design shape. When the prediction error has a significant influence on the result, the DOE method should be applied, e.g., centered composite designs (CCD), face-centered cubic designs, factorial designs. As the noise is not significant, it is possible to use Latin-hypercube sampling (LHS), minimum bias designs, and orthogonal arrays (OAs) methods. Article [13] introduced a few designs of experiment techniques and guidelines used to search for sampling methods.

The selection of the metamodel that connects the generated measurement points is also significant. The most popular surrogate models are polynomial response surfaces, Kriging; gradient-enhanced Kriging (GEK); the radial basis function; artificial neural networks, and Bayesian networks. The polynomial metamodel referred to as a response surface model is a set of statistical and mathematical methods. The models are developed using regression, which is the process of fitting a regression model  $y = s(x, \beta) + \varepsilon$  to a dataset of  $n$  variable settings  $x_i$  and corresponding responses  $y_i$ . The least-squares method chooses the regression coefficients  $\beta$  so that the quadratic error is minimized

$$\min \sum_{i=1}^n \varepsilon_i^2 = \sum_{i=1}^n (y_i - s(x_i, \beta))^2. \quad (1)$$

For example, the second-order polynomial models can be used to fit a metamodel in  $k$  design variables:

$$y = s(x, \beta) + \varepsilon = \beta_0 + \sum_{i=1}^k \beta_i x_i + \sum_{i=1}^{k-1} \sum_{i < j=2}^k \beta_{ij} x_i x_j + \varepsilon. \quad (2)$$

More information about this method and mathematical explanation can be found in [14]. The polynomial response method is easy to construct, cheap to work with, but in some cases less accurate than the other methods for high-order nonlinear problems. For low-order nonlinear and small-scale problems, the polynomial model performs best in terms of both average accuracy and robustness, which was presented in [15]. In DesignXplorer, non-parametric regression (NPR) is a method based on the Support Vector Machine classification theorem. The non-parametric regression metamodel categorizes the noisy data and uses only those that reflect the outputs the best. This approach utilizes all the main features that characterize the maximal margin algorithm. Non-parametric regression systems with nonlinear responses and noisy results can be described as below:

$$f(x) = \langle w, x \rangle + b, \quad (3)$$

where  $f(x)$  is the response of interest,  $w$  and  $b$  are mathematically defined as:

$$w = \sum_{i=1}^n (\alpha_i^* - \alpha_i) \varphi(x_i), \quad (4)$$

$$b = \frac{1}{2} \langle w, (x_r + x_s) \rangle, \quad (5)$$

where  $\alpha_i^*$ ,  $\alpha_i$  are Lagrange variables, and  $x_r$ ,  $x_s$  are support vectors [16].

The Kriging algorithm, which is a combination of a polynomial model and localized deviations can be described as:

$$y(x) = f(x) + Z(x), \quad (6)$$

where  $y(x)$  is the function of interest,  $f(x)$  is a polynomial function of  $x$ , and  $Z(x)$  is interpolations of the  $N$  sample data points. The covariance matrix of  $Z(x)$  is given by:

$$\text{Cov}[Z(x^i), Z(x^j)] = \sigma^2 R([r(x^i, x^j)]), \quad (7)$$

where  $R$  is the correlation matrix, and  $r(x^i, x^j)$  is the spatial correlation of the function between any two of the  $N$  samples  $x^i$  and  $x^j$ . The correlation function is given by:

$$r(x^i, x^j) = \exp \left( - \sum_{k=1}^M \theta_k |x_k^i - x_k^j|^2 \right), \quad (8)$$

$\theta_k$  are unknown parameters of fit,  $M$  is the number of design variables, and  $x_k^i$  and  $x_k^j$  are  $k$ -th components of sample points [17].

A metamodel uses simple functions to approximate more difficult objectives based on a limited amount of data  $x_1, x_2, \dots, x_n$ . The metamodel can be built to approximate the true response as:

$$\hat{y} = s(x), \quad (9)$$

where  $s(x)$  is the mathematical function defining the metamodel, which maps the design variables  $x$  to the predicted response  $\hat{y}$ . In general, this approximation is not exact, and the predicted response  $\hat{y}$  will differ from the observed response  $y$  from the detailed model.

The prediction of the simulation-based model output can be defined as:

$$f(x) = \hat{f}(x) + \varepsilon(x) = s(x) + \varepsilon(x), \quad (10)$$

where the error  $\varepsilon$  consequently represents the approximation error.

A metamodel for a single response is built from a dataset of input  $x_i$  and corresponding output  $y_i = f(x_i)$ , where  $i = [1, \dots, n]$  and  $n$  is the number of designs used to fit the model. Consequently,  $n$  evaluations of the detailed model with different variable settings  $x_i = (x_1, x_2, \dots, x_k)^T$  of the  $k$  design variables are required to build the metamodel [18, 19].

Choosing the optimal design among multiple objective functions is challenging. In general, a multi-objective optimization problem is formulated as:

$$\min / \max f_i(x) \quad i = 1, \dots, N_{\text{obj}}. \quad (11)$$

Subject to:

$$\begin{cases} g_j(x) = 0, & j = 1, \dots, M, \\ h_k(x) \leq 0, & k = 1, \dots, K, \end{cases} \quad (12)$$

where  $f_i$  is the  $i$ -th objective function;  $x$  is the decision vector that presents a solution;  $N_{\text{obj}}$  is the number of objectives;  $M$  and  $K$  are the numbers of equality and inequality constraints [20]. Multi-objective genetic algorithm (MOGA) is a variant of the popular non-dominated sorted genetic algorithm-II (NSGA-II). Genetic algorithms (GA) are classified in metaheuristic methods, which aim to find an acceptable solution in very complex optimization and search problems [21].

In this study, the multi-objective optimization of a butterfly valve using the fluid-structure interaction (FSI) metamodel was performed. The objective function was to maximize the flow rate coefficient and to minimize the mass of the valve disc.

The paper is organized as follows. The most important information about the butterfly valve operation and design is presented in Sec. 2. The numerical

simulation of the fluid flow through the valve and the pressure effect on the valve components are presented in Sec. 3. The description of the butterfly valve optimization process and a brief explanation of the methods used are presented in Sec. 4. The results and discussion are presented in Sec. 5. Section 6 focuses on the conclusions. Finally, Sec. 7 contains conclusions with recommendations for the future work.

## 2. THE METAMODEL OF A BUTTERFLY VALVE

### 2.1. Butterfly valve: construction and operation

The basic elements of the butterfly valve are disk, stem, body, bearings, actuator. A part that has a direct impact on the flow of the medium is the disk. Mounted on the stem can rotate 90 degrees, thereby completely opening or closing the flow (in position  $0^\circ$ ). With this device, it is also possible to regulate the flow rate depending on the opening degree of the valve. Although the values of the flow coefficient and the forces acting on the surface of the disk depend on the opening angle, all presented results in this article refer to an angle of 70 degrees. There are a few different types of butterfly valves on the market, including the zero offset known as a concentric design, double offset, and triple offset. An appropriate construction or plastic/rubber sealing prevent leakage. The basic parameters of the materials used in the study are presented in Table 1.

TABLE 1. Specifications of the butterfly valve.

Operating temperature of the fluid (water)	20°C
Fluid density	998.2 kg/m <sup>3</sup>
Disc material	X2CrNiMo17-12-2
Solid density	7980 kg/m <sup>3</sup>
Inlet pressure	$0.2 \cdot 10^6$ Pa
Outlet pressure	$0.1 \cdot 10^6$ Pa

The geometry of the examined object was created using the SpaceClaim. A special script was written that automatically provided geometry for analysis. Scripting in the SpaceClaim environment uses IronPython. The butterfly valve disk structure consists of simple symmetrical elements that are an advantage in the creation of a CAD object. The script contains commands for drawing objects, rotation, extension, rounding, also selection commands to make surfaces for a boundary condition. Examples of the IronPhyton script are shown as follows:

```

# Sketch Rectangle
point1 = Point2D.Create(MM(Parameters.D1_obl_2),MM(Parameters.Width_body_2))
point2 = Point2D.Create(MM(Parameters.L1_obl_2),MM(Parameters.Width_body_2))
point3 = Point2D.Create(MM(Parameters.L1_obl_2),MM(-Parameters.Width_body_2))
result = SketchRectangle.Create(point1, point2, point3)
# EndBlock

# Revolve 1 Face
selection = Selection.Create(GetRootPart().Bodies[1].Faces[0])
axisSelection = Selection.Create(GetRootPart().DatumLines[0])
axis = RevolveFaces.GetAxisFromSelection(selection, axisSelection)
options = RevolveFaceOptions()
options.ExtrudeType = ExtrudeType.ForceIndependent
result = RevolveFaces.Execute(selection, axis, DEG(360), options)
# EndBlock

```

### 3. METHODS

#### 3.1. Input parameters bound

The initial dimensions of the examined object were created based on solutions proposed by manufacturers. They are only an introduction to further considerations. For the valve with a nominal diameter of 50 mm, an optimization process was carried out in which the fixed dimensions were: FI; An; Wd; DN; ThB, and the variable parameters were R1; R2; ThP\_2\_2. Both the fixed and the bound variable parameters are presented in Table 2.

TABLE 2. Value of fixed and variable dimensions.

Fixed dimensions	Value
DN	50 mm
Wd	55 mm
ThB	3 mm
ThP_1	1 mm
FI	12.5 mm
An	70°
Variable dimensions	Range
R1	0.1 mm $\leq$ R1 $\leq$ 1 mm
R2	0.1 mm $\leq$ R2 $\leq$ 45 mm
ThP_2_2	1 mm $\leq$ Thick_plate $\leq$ 6 mm

As a result of the working script, a butterfly valve was assembled with inlet and outlet channels. The pressure differences were measured on the valve and

the channels in the analysis were flow-stabilizing. A fluid domain was introduced between the inlet and the outlet, on which further CFD calculations were based. The explanation of the valve dimensions, channel length, and disc thickness are presented in the drawings below (Figs 1 and 2).

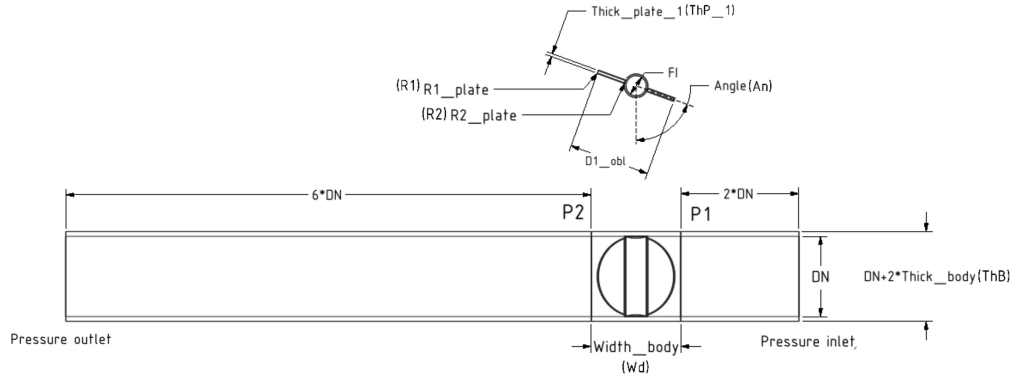


FIG. 1. Dimensions of the butterfly valve.

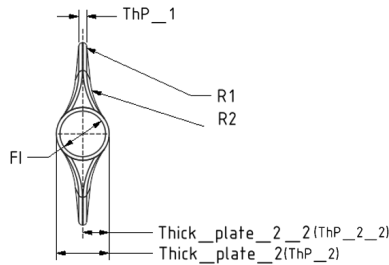


FIG. 2. Explanation of the designation used in the valve's description.

### 3.2. Fluid flow analysis

To meet system requirements and adequately select the valve for the task and installation, it is necessary to know the fluid rate related to the opening of the valve. For the correct operation of the device, it is recommended to avoid using the disk in extreme positions, which may result in unstable operation of the system. Depending on what unit system is used, the flow coefficient can be described as:

$$KV = Q \sqrt{\frac{\Delta P_{\text{Ref}} \cdot \rho_{\text{Ref}}}{\Delta P \cdot \rho}}, \quad (13)$$

where  $KV$  – flow coefficient [ $\text{m}^3/\text{h}$ ],  $Q$  – flow rate [ $\text{m}^3/\text{h}$ ],  $\Delta P_{\text{Ref}} = 1$  [bar] – reference pressure drop,  $\Delta P$  – pressure drop across the valve [ $P_1 - P_2$ ] [bar],  $\rho_{\text{Ref}} = 1000$  [ $\text{kg}/\text{m}^3$ ] – reference density of water,  $\rho$  – water density [ $\text{kg}/\text{m}^3$ ].

The location of each valve should be at an appropriate distance from the source of the disturbance (e.g., pumps, elbows). The influence of the stabilizing pipe on the results was also shown in [2]. To solve this problem and also comply with the computing requirements, an upstream pipe equal to twice the length of the diameter and a downstream pipe with the length equal to six times the length of the diameter were introduced. The numerical grid was composed of tetrahedral elements. Calculations used the  $k$ - $\epsilon$  turbulence model due to its wide application but also small computational requirements.

To meet the requirements of numerical calculations of fluid dynamics, but also to reduce the calculation error, a numerical mesh independence test was performed (see Table 3). For this purpose, the values of the KV parameter were compared depending on the numerical grid used. The values of the  $y^+$  parameter were also checked, which is a dimensionless parameter and describes the distance from the wall to the first mesh node. In the case of using the  $k$ - $\epsilon$  turbulence model, only those meshes with the value of  $y^+$  within the range  $30 < y^+ > 300$  were taken into consideration. The parameters of grid number 5 were used in the further simulations.

TABLE 3. Mesh independence parameters.

No.	Element order	Elements	KV [m <sup>3</sup> /h]	$y^+$	Comments
1	Linear	29057	98.20	21812	Without inflation
2	Linear	523137	82.89	433	Inflation
3	Linear	215657	83.02	119	Sweep/Inflation
4	Quadratic	300857	83.21	76	Sweep/Inflation/Sizing – 0.001
5	Quadratic	760228	83.58	39	Sweep/Inflation/Sizing – 0.0005
6	Quadratic	2609944	82.24	20	Sweep/Inflation/Sizing – 0.00025
7	Quadratic	4062521	82.54	15	Sweep/Inflation/Sizing – 0.0002

For the initial conditions, the pressure drop between the inlet and outlet was determined as indicated by the standard describing the methodology for conducting this type of testing [22]. As shown in Fig. 3, the results obtained for the computer simulation are consistent with the values presented by the manufacturers. In particular, the simulation result coincides with the data of manufacturer No. 3. The two other data sets differ slightly from the simulation results. In the 70–90 degree of opening, the results of manufacturer No. 1 and 2 are much higher since each manufacturer uses a different disk geometry.

The multi-objective optimization procedure was prepared using ANSYS Project Schematic graphic interface. Figure 4 shows the diagram of fluid-structure interaction components in the Ansys program. The stress analysis occurring during the flow of the medium through the butterfly valve was carried out, and

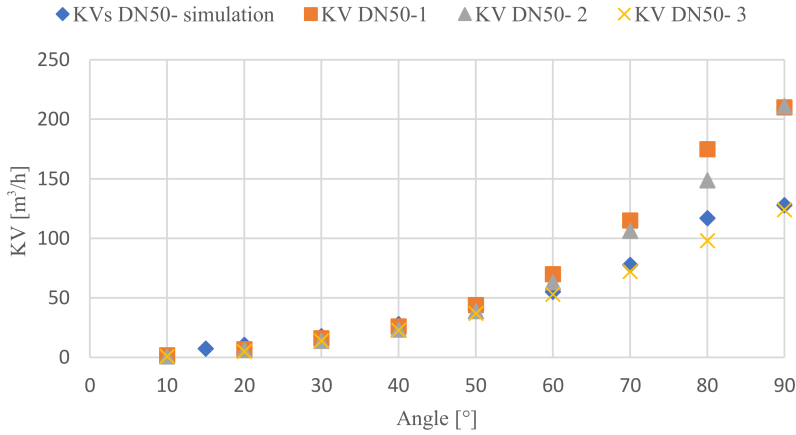


FIG. 3. Examples of the flow rate coefficient for butterfly valves from different manufacturers against computational data.

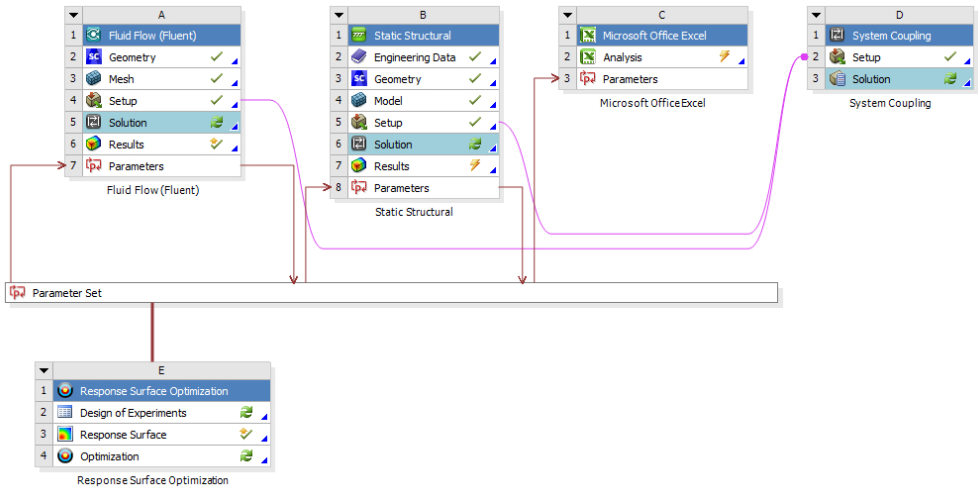


FIG. 4. The multi-objective optimization procedure.

the yield stress of 240 MPa (for X2CrNiMo17-12-2 material) was accepted as a constraint of optimization.

### 3.3. Optimization procedure

In the first instance, a simple face-centered CCD method was used. It is built for the second-order response surface model. The minimum number of design points in CCD with three variables is 15 ( $2^k + 2k + 1$ ). However, when the number of variables increases, computing time also is considerably high. The CCD

method seems to be appropriate for a small number of variables. Nevertheless, taking into account the range of R2's values and impact on geometry, the CCD enhanced method was chosen. As a result, the final number of measurement points reached 29. Based on the measurement points, metamodels were generated, the differences of which are best observed by comparing the response surfaces. Full second-order polynomials, non-parametric regression, Kriging methods were investigated. Next, multi-objective MOGA optimizations were used. In this research, the multi-objective function is to maximize the flow rate coefficient and to minimize the mass of the valve disc. Thus, based on the general description of multi-objective optimization (Eqs (11) and (12)), in this research, the solution procedure goes as follows:

$$\min f(x) = \{\text{mass}\}, \quad (14)$$

$$\max f(x) = \{\text{KV}\}, \quad (15)$$

where

$$x = [R1, R2, \text{ThP\_2\_2}]. \quad (16)$$

MOGA's parameters were set to generate 3000 samples initially, 600 samples per iteration in a maximum of 20 iterations with one candidate point. Mutation probability was equal to 0.01 and crossover probability equal to 0.98.

#### 4. RESULTS

Fluid flow analysis provides information about the pressure field and, more importantly, allows determining the valve KV coefficient, which is calculated according to Eq. (13) and with the guidelines contained in the chapter Fluid flow analysis. A disk shape has a significant impact on the pressure field. The increasing of radius R2 or ThP\_2\_2 results in smoother pressure transitions around the disk (see Fig. 5). Also, the issue that causes the most problems in the valve's work is cavitation. It affects increased noise and often results in damage to the device. It is worth noting that information about the pressure exerted on the element can be transferred to structural analysis. This happens in fluid-structure interaction (FSI) where pressure is transferred to other systems. These loads may cause structural deformation significant enough to change the fluid flow itself.

In Fig. 6, local sensibility can be noticed. The R1 has the most significant impact on of the KV coefficient level, but the small range of variables for this parameter has little scope for change. An increase in ThP\_2\_2 also expands the value of KV. The biggest influence on mass is due to the largest size range of ThP\_2\_2 and R2 parameters.

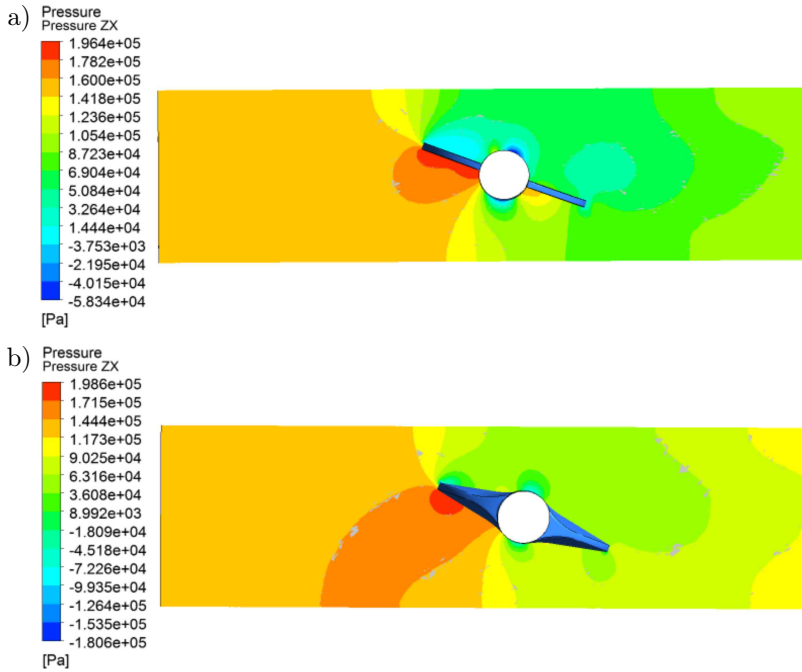


FIG. 5. Pressure contour for valve dimensions: a)  $ThP_{2_2} = 1$  mm,  $R1 = 0.1$  mm,  $R2 = 0.1$  mm at the middle plane and 70 degree opening, b)  $ThP_{2_2} = 6$  mm,  $R1 = 0.55$  mm,  $R2 = 22.55$  mm.

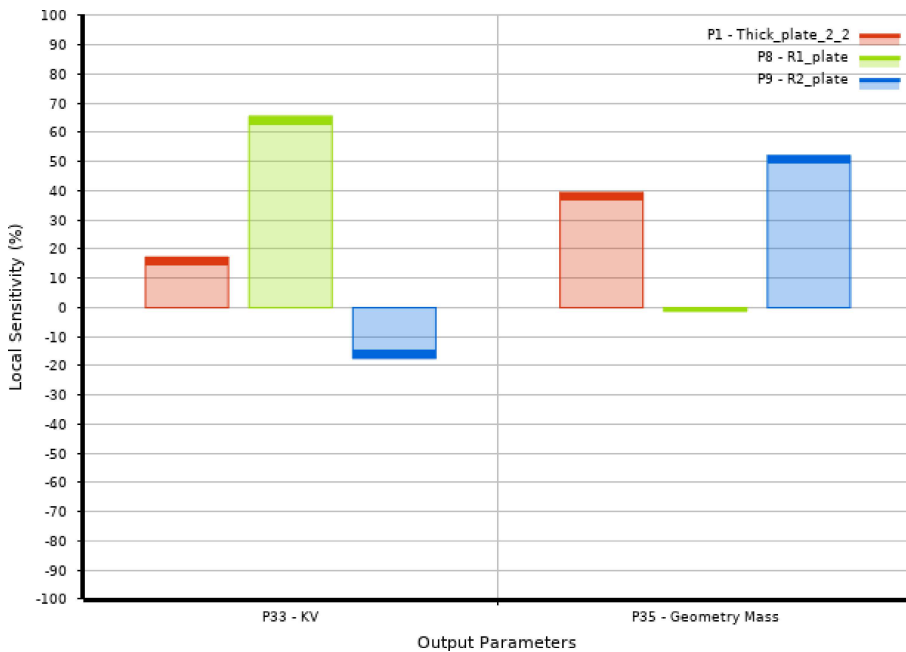


FIG. 6. Local sensitivity analysis.

TABLE 4. Design parameters and optimization objectives.

No.	Variables			Objectives	
	ThP_2_2 [mm]	R1 [mm]	R2 [mm]	KV [m <sup>3</sup> /h]	Mass [kg]
1	3.50	0.550	22.550	98.56	0.0601
2	1.00	0.550	22.550	97.11	0.0540
3	2.25	0.550	22.550	101.93	0.0567
4	6.00	0.550	22.550	102.22	0.0694
5	4.75	0.550	22.550	104.76	0.0643
6	3.50	0.100	22.550	82.40	0.0602
7	3.50	0.325	22.550	91.12	0.0602
8	3.50	1.000	22.550	117.35	0.0599
9	3.50	0.775	22.550	102.95	0.0600
10	3.50	0.550	0.100	101.94	0.0491
11	3.50	0.550	11.325	111.58	0.0543
12	3.50	0.550	45.000	93.68	0.0692
13	3.50	0.550	33.775	98.63	0.0650
14	1.00	0.100	0.100	83.58	0.0363
15	2.25	0.325	11.325	92.12	0.0493
16	6.00	0.100	0.100	86.51	0.0629
17	4.75	0.325	11.325	98.63	0.0599
18	1.00	1.000	0.100	105.89	0.0358
19	2.25	0.775	11.325	112.89	0.0491
20	6.00	1.000	0.100	113.71	0.0627
21	4.75	0.775	11.325	110.56	0.0598
22	1.00	0.100	45.000	77.80	0.0693
23	2.25	0.325	33.775	89.32	0.0632
24	6.00	0.100	45.000	83.17	0.0746
25	4.75	0.325	33.775	92.34	0.0681
26	1.00	1.000	45.000	95.56	0.0689
27	2.25	0.775	33.775	97.56	0.0630
28	6.00	1.000	45.000	95.64	0.0743
29	4.75	0.775	33.775	99.40	0.0679

Graphical representation of the metamodel on the KV value with R2 and ThP\_2\_2 is presented in this paper. As shown in Fig. 7, the simulation points do not always coincide with the plot surface. Metamodel compatibility parameters and some measurement errors are shown in Table 5. The Kriging method gives the best matching to the measuring points, but its finite number does not consider the whole measuring range (especially with CCD). Slightly better matching can be seen for non-parametric regression than full second-order polynomials.

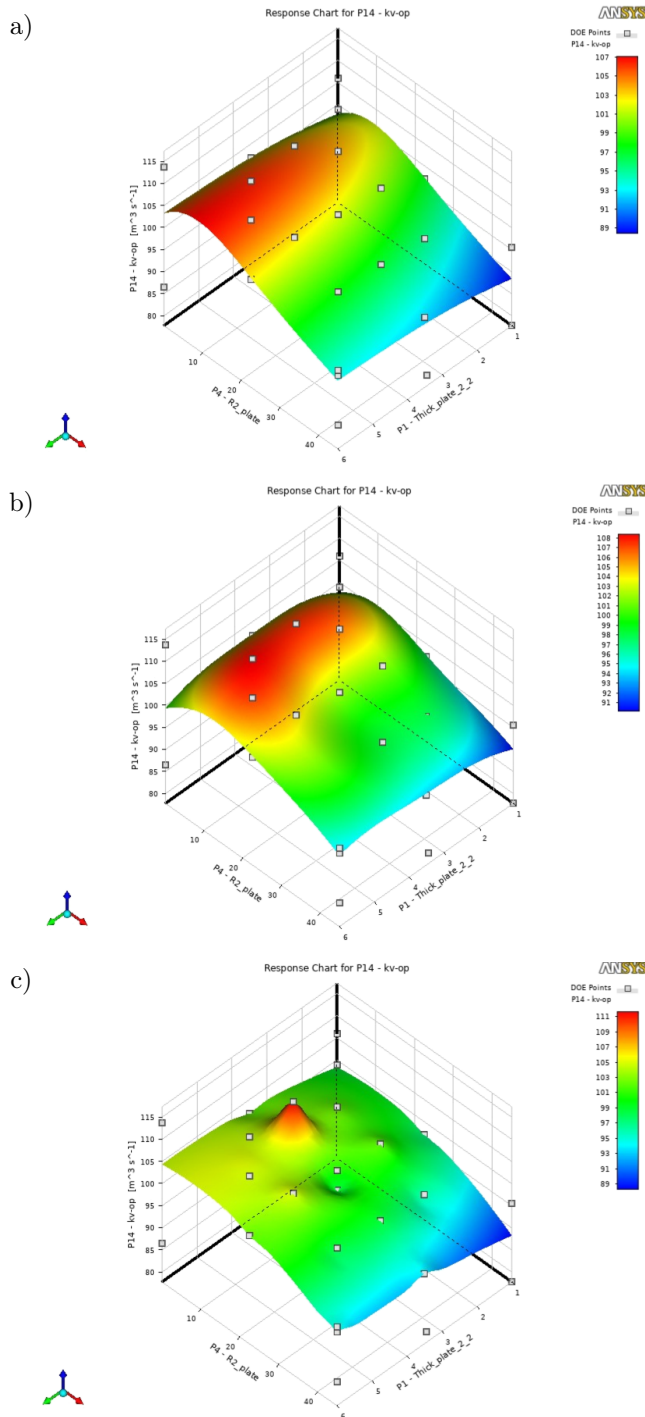


FIG. 7. Graphical representation of KV, R2, ThP\_2\_2 parameters response chart plots for:  
a) full second-order polynomials, b) non-parametric regression, c) Kriging.

TABLE 5. Metamodel compatibility parameters.

	Root mean square error				Relative maximum absolute error				Relative average absolute error			
	Learning points		Verification points		Learning points		Verification points		Learning points		Verification points	
	KV	Mass	KV	Mass	KV	Mass	KV	Mass	KV	Mass	KV	Mass
Full second-order polynomials	2.87	0.0001	2.93	0.0001	64.11	5.42	66.22	5.49	21.40	1.48	22.68	1.46
Non-parametric regression	0.96	0.0003	1.00	0.0003	39.85	4.228	41.17	4.27	5.46	3.35	5.80	3.44
Kriging	0	0	0	0	0	0	0	0	0	0	0	0

The Kriging method best reflects high deviations and may be used as a guide in further studies. Growth in the number of simulation points could increase the accuracy of the metamodel, but this is associated with a longer duration of the process. Furthermore, with such a small number of variables, the number of DOE points is not significant. However, with their increase, changing methods of generating experimental points and metamodeling methods should be considered.

Metamodels presented in graphic form are represented in the form of equations, and for the full second-order polynomials are described as:

$$\begin{aligned}
 \text{KV} = & 72.59 + 3.67\text{ThP}_{\_2\_2} + 51.5\text{R1} + 0.249\text{R2} - 0.342\text{ThP}_{\_2\_2} \\
 & \times \text{ThP}_{\_2\_2} - 16.9\text{R1} \times \text{R1} - 0.00688\text{R2} \times \text{R2} - 0.3\text{ThP}_{\_2\_2} \\
 & \times \text{R1} - 0.0108\text{ThP}_{\_2\_2} \times \text{R2} - 0.275\text{R1} \times \text{R2}, \quad (17)
 \end{aligned}$$

$$\begin{aligned}
 \text{Mass} = & 0.032731 + 0.003492\text{ThP}_{\_2\_2} - 0.00021\text{R1} + 0.000911\text{R2} \\
 & + 0.000261\text{ThP}_{\_2\_2} \times \text{ThP}_{\_2\_2} - 0.00029\text{R1} \times \text{R1} \\
 & - 0.000002\text{R2} \times \text{R2} + 0.000035\text{ThP}_{\_2\_2} \times \text{R1} \\
 & - 0.000096\text{ThP}_{\_2\_2} \times \text{R2} + 0.000001\text{R1} \times \text{R2}. \quad (18)
 \end{aligned}$$

The R-squared (R<sup>2</sup>) parameter describing the fit of the metamodel to the input data for the KV is 89.57% and for mass 99.9%.

Sets of Pareto fronts based on different metamodels are presented in Fig. 8. Their shape differs from each other, which is directly related to the methods used. Pareto fronts present only the best possible options for solving the goals under consideration. The process of metamodeling and optimization led to the following results in the form of one candidate in each metamodel presented in Table 6. Optimal candidate points, selected in the optimization process, were placed on the Pareto front chart.

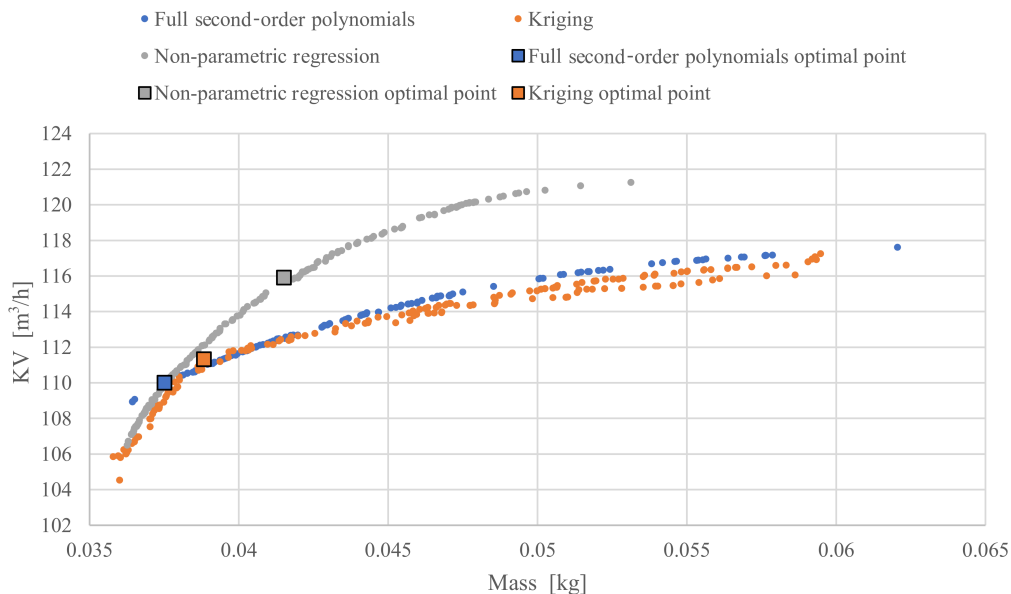


FIG. 8. Pareto fronts for different metamodels.

TABLE 6. Optimal candidates for different metamodels.

	Full second-order polynomials	Non-parametric regression	Kriging
ThP_2_2 [mm]	1.040	1.820	1.910
R1 [mm]	0.990	0.990	0.990
R2 [mm]	1.980	7.140	5.120
KV [m <sup>3</sup> /h]	110.730	116.300	112.150
Mass [kg]	0.036	0.041	0.039

Optimal point parameters did not differ significantly from each other. The R1 value was close to 1 mm. The ThP\_2\_2 parameter varies from 1 mm to 1.9 mm. The parameter R2 has the widest range (1.98 mm to 7.14 mm). In all

cases, the obtained KV coefficient value was above  $108 \text{ m}^3/\text{h}$ , and the disk weight varied from  $0.036\text{--}0.041 \text{ kg}$ . All candidates were verified in the CFD simulation to check metamodels' correctness.

The next step was to check the stress in the disk stricture caused by the fluid flow. The scheme of the procedure is presented in Fig. 4. Taking into account the safety issues, FSI analyses were performed for the higher parameters: pressure inlet  $1.6 \times 10^6 \text{ Pa}$  and pressure outlet  $0 \text{ Pa}$ . The analysis of the results between the initial geometry and the optimized geometry did not reveal any significant differences in the level or areas of the highest stresses. In the case of the optimal design, the stress fields are more homogeneous than in the initial version, which was characterized by the highest stresses in sharp areas without rounds. The drop in the maximum von Mises stress can be observed for  $90^\circ$ ,  $80^\circ$  and  $10\text{--}40^\circ$  open positions. For both structures, the stress constraint was not exceeded. The maximum stresses obtained on the disk when changing the disk position are presented in Table 7.

TABLE 7. Maximum disc stresses value.

Initial		Kriging's optimal	
Angle [ $^\circ$ ]	Max. stress [Pa]	Angle [ $^\circ$ ]	Max. stress [Pa]
90	2.25E+07	90	6.82E+06
80	4.76E+08	80	1.31E+08
70	1.24E+07	70	1.99E+08
60	3.31E+07	60	1.99E+08
50	1.50E+08	50	1.59E+08
40	4.57E+08	40	1.32E+08
30	1.79E+07	30	1.12E+08
20	1.87E+08	20	1.00E+08
10	1.27E+08	10	1.06E+08

The von Mises stress for the initial and optimal geometry is shown in Figs 9 and 10. The highest level of stress can be observed at the connection between the stem mounting and the disk.

Considering the small differences between the R1 and ThP\_2\_2 values, proposed in the optimization process by different metamodels, the R2 parameter was of the greatest importance. Introducing the radius between the shaft mounting and the disk, significantly reduces the level of stress concentration (from  $455 \times 10^6 \text{ Pa}$  to  $198 \times 10^6 \text{ Pa}$ ), resulting in a uniform field distribution and reduction of the maximum stress values. In any of the above cases, the values of hazardous stresses were not exceeded. Compared to the initial design, the maximum stresses ( $141 \times 10^6 \text{ Pa}$ ) increased slightly, thus remarkably improving the flow coefficient.

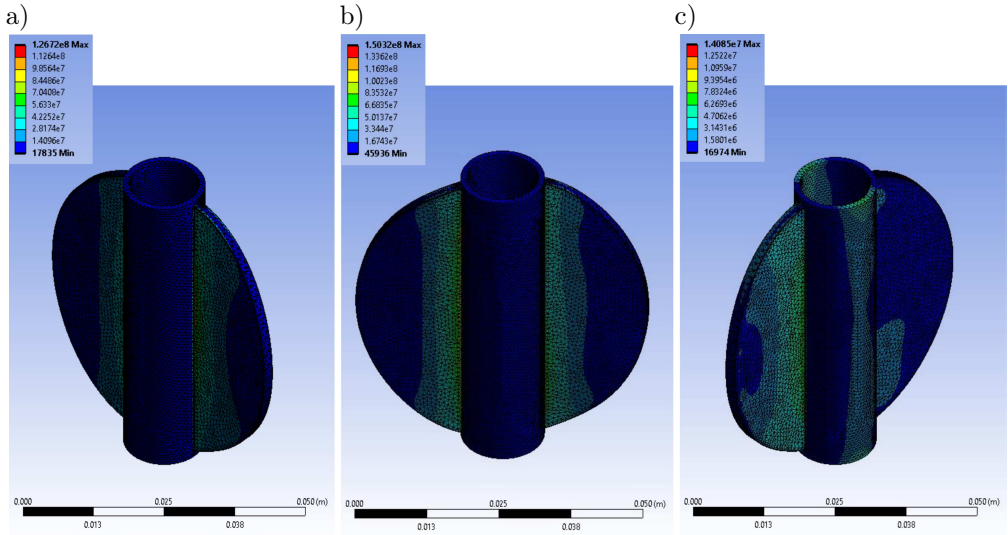


FIG. 9. Equivalent von Mises stress for initial disc geometry and opening angle: a)  $10^\circ$ , b)  $50^\circ$ , c)  $80^\circ$ .

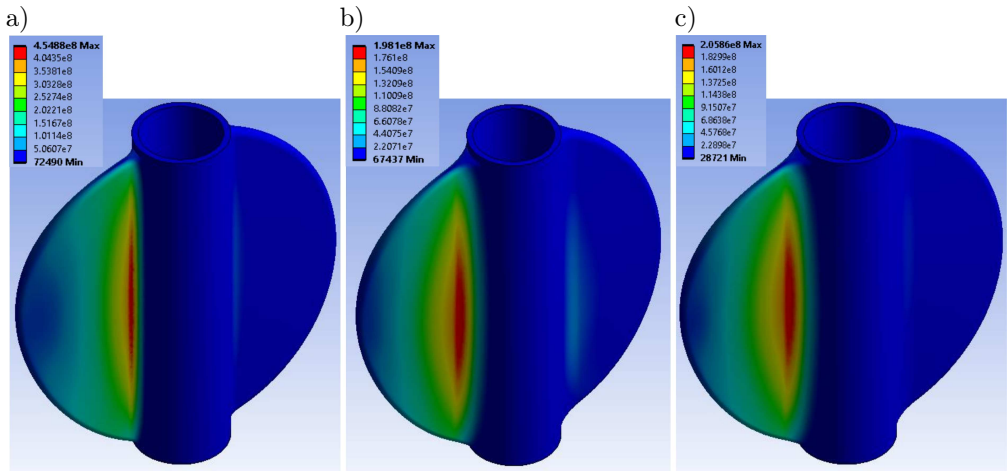


FIG. 10. Equivalent von Mises stress for optimal candidates: a) full second-order polynomials, b) non-parametric regression, c) Kriging.

## 5. DISCUSSION

The results for the initial, optimal, and verification parameters are listed in Table 8. It can be seen that despite a significant improvement in the rate of the KV coefficient, their values are not confirmed at the verification point. Against the uncertainty as to the methods used, the best results were shown by the Kriging method. The error between metamodel predictions and the candidate's simulation was 3% for KV and 1% for geometry mass.

TABLE 8. Result comparison.

	KV [m <sup>3</sup> /h]	Mass [kg]
Initial	83.58	0.0362
Optimal		
Full second-order polynomials	110.73	0.036
Non-parametric regression	116.30	0.041
Kriging	112.15	0.039
Verification		
Full second-order polynomials	104.13	0.0375
Non-parametric regression	119.03	0.0441
Kriging	115.27	0.0430
Error [%]		
Full second-order polynomials	6%	3%
Non-parametric regression	2%	4%
Kriging	3%	1%

Weak metamodel matching can be seen for full second-order polynomials and non-parametric regression. Relative maximum absolute error (KV) for those methods are slightly high (66.22% and 41.17%, respectively in Table 6) as to the continuity disturbances of the valve model behaviour. The difference between the values obtained by simulation and the metamodeling prediction is below 10%. Although the results may seem satisfactory, their geometry was in an area well represented by each of the metamodels, which does not mean that the entire studied area is well described. The best concordance was obtained for the predicted mass of the object. The metamodel performed well for the predicting mass value.

## 6. CONCLUSIONS

Our aim of the work was to find the metamodeling methodology for the multi-objective optimization of fluid flow machines. The methods used the FSI analysis at defined design points to evaluate the KV coefficient as well as structural stress. Furthermore, optimization of the valve was carried out by using the following modelling algorithms:

- CCD with full second-order polynomials,
- non-parametric regression,
- and Kriging model.

Moreover, the multi-objective genetic algorithm optimization procedure was applied to reduce the weight of the valve disc as well as to maximize the KV

coefficient. Optimization allowed to improve the KV value by 37.6%. However, this caused an increase in disk mass (0.002 kg) from the optimal valve geometry when compared to initial dimensions. Verification of the optimal point, to check the correctness of the selected metamodel, showed a 3% error between optimal and verification KV coefficient values. The created metamodel can be easily used as an input parameter to the next element of the system. In the case of a butterfly valve, the KV coefficient is only a part of the entire hydraulic system, and the choice of the internal components or an opening angle has a critical effect on other units. Optimization of the structure resulted in KV improvement, homogenization, and a decrease in disk stress at maximum and minimum positions.

The described metamodeling methods have applications in bioengineering. In the future, our research group plans to implement them in the construction of artificial heart support chambers.

## Funding

This research did not receive any special grant from funding agencies in the public, commercial, or not-for-profit sectors.

## Declaration of Competing Interest

The authors declare that they have no known competing financial interests or personal relationships that could have appeared to influence the work reported in this paper.

## REFERENCES

1. M.M. Said, H.S.S. Abdelmeguid, L.H. Rabie, The accuracy degree of CFD turbulence models for butterfly valve flow coefficient prediction, *American Journal of Industrial Engineering*, **4**(1): 14–20, **2016**, doi: 10.12691/ajie-4-1-3.
2. X.-M. Zhou, Z.-K. Wang, Y.-F. Zhang, A simple method for high-precision evaluation of valve flow coefficient by computational fluid dynamics simulation, *Advances in Mechanical Engineering*, **9**, Article ID: 1687814017713702, 2017, doi: 10.1177/1687814017713702.
3. M.I. Al-Amayreh, M.I. Kilani, A.S. Al-Salaymeh, Numerical study of a butterfly valve for vibration analysis and reduction, *International Journal of Mechanical, Aerospace, Industrial, Mechatronic and Manufacturing Engineering*, **8**(12): 1970–1974, 2014.
4. M. Charlebois-Ménard, M. Sanjosé, A. Marsan, A. Chauvin, Y. Pasco, S. Moreau, M. Brouillette, Experimental and numerical study of the noise generation in an out-flow butterfly valve, [in:] 21st AIAA/CEAS Aeroacoustics Conference, 22–26 June, 2015, Dallas, TX, doi: 10.2514/6.2015-3123.
5. X. Song, L. Wang, Y. Park, Fluid and structural analysis of a large diameter butterfly valve, *Journal of Advanced Manufacturing Systems*, **8**(1): 81–88, 2009, doi: 10.1142/S0219686709001663.

6. S.Y. Jeon, J.Y. Yoon, M.S. Shin, Flow characteristics and performance evaluation of butterfly valves using numerical analysis, *IOP Conference Series: Earth and Environmental Science*, **12**(1): 012099, 6 pp., 2010, doi: 10.1088/1755-1315/12/1/012099.
7. F. Vakili-Tahami, M. Zehsaz, M. Mohammadpour, A. Vakili-Tahami, Analysis of the hydrodynamic torque effects on large size butterfly valves and comparing results with AWWA C504 standard recommendations, *Journal of Mechanical Science and Technology*, **26**(9): 2799–2806, 2012, doi: 10.1007/s12206-012-0733-8.
8. R. Kasukurthy, P.S. Challa, R.R. Palanikumar, B.R. Manimaran, D. Agonafer, Flow analysis and linearization of rectangular butterfly valve flow control device for liquid cooling, [in:] 17th IEEE Intersociety Conference on Thermal and Thermomechanical Phenomena in Electronic Systems (I Therm), 29 May – 1 June, 2018, San Diego, CA, USA, pp. 683–687, doi: 10.1109/ITHERM.2018.8419503.
9. X.G. Song, L. Wang, Y.C. Park, Analysis and optimization of a butterfly valve disc, *Proceedings of the Institution of Mechanical Engineers, Part E: Journal of Process Mechanical Engineering*, **223**(2): 81–89, 2009, doi: 10.1243/09544089JPME236.
10. X.G. Song, L. Wang, S.H. Baek, Y.C. Park, Multidisciplinary optimization of a butterfly valve, *ISA Transactions*, **48**(3): 370–377, 2009, doi: 10.1016/j.isatra.2009.01.009.
11. S. Corbera, J. Luis, J. Antonio, Multi-objective global optimization of a butterfly valve using genetic algorithms, *ISA Transactions*, **63**: 401–412, 2016, doi: 10.1016/j.isatra.2016.03.008.
12. B. Durakovic, Design of experiments application, concepts, examples: State of the art, *Periodicals of Engineering and Natural Sciences*, **5**(3): 421–439, 2017, doi: 10.21533/pen.v5i3.145.
13. Y. Mack, T. Goel, W. Shyy, R. Haftka, Surrogate model-based optimization framework: A case study in aerospace design, [in:] *Evolutionary Computation in Dynamic and Uncertain Environments*, S. Yang, Y.-S. Ong, Y. Jin [Eds], Springer, Berlin Heidelberg, 2007, pp. 323–342, doi: 10.1007/978-3-540-49774-5\_14.
14. A.-B. Ryberg, R. Bäckryd, L. Nilsson, *Metamodel-Based Multidisciplinary Design Optimization for Automotive Applications*, Technical Report LIU-IEI-R-12/003, Linköping University, 2012.
15. R. Jin, W. Chen, T.W. Simpson, Comparative studies of metamodeling techniques under multiple modeling criteria, *Structural and Multidisciplinary Optimization*, **23**: 1–13, 2001, doi: 10.1007/s00158-001-0160-4.
16. P. Sofotasiou, B. Hughes, S.A. Ghani, CFD optimisation of a stadium roof geometry: a qualitative study to improve the wind microenvironment, *Sustainable Buildings*, **2**, Article No. 8, 2017, doi: 10.1051/sbuild/2017006.
17. DesignXplorer 19.2/DesignXplorer User’s Guide/DesignXplorer Theory/Response Surface Theory/Kriging Algorithms, ANSYS, Inc. (n.d.).
18. S. Dasari, A. Cheddad, P. Andersson, Predictive modelling to support sensitivity analysis for robust design in aerospace engineering, *Structural and Multidisciplinary Optimization*, **61**: 2177–2192, 2019, doi: 10.1007/s00158-019-02467-5.
19. A.I. Khuri, S. Mukhopadhyay, Response surface methodology, *WIREs Computational Statistics*, **2**(2): 128–149, 2010, doi: 10.1002/wics.73.

20. J.P. Roselyn, D. Devaraj, S.S. Dash, Multi-Objective Genetic Algorithm for voltage stability enhancement using rescheduling and FACTS devices, *Ain Shams Engineering Journal*, **5**(3): 789–801, 2014, doi: 10.1016/j.asej.2014.04.004.
21. M. Tabassum, K. Mathew, A genetic algorithm analysis towards optimization solutions, *International Journal of Digital Information and Wireless Communications*, **4**(1): 124–142, 2014, doi: 10.17781/P001091.
22. PN-EN 60534-2-1:2011/AC1, Industrial-process control valves – Part 2-1: Flow capacity – Sizing equations for fluid flow under installed conditions, Polski Komitet Normalizacyjny, Warszawa, 2015.

*Received November 18, 2020; revised version March 8, 2021.*